PCCP
Physical Chemistry Chemical Physics

Accepted Manuscript

This article can be cited before page numbers have been issued, to do this please use: S. Choi, H. Bong, K. Kim, S. Jeon and J. Oh, *Phys. Chem. Chem. Phys.*, 2026, DOI: 10.1039/D5CP04347F.

ROYAL SOCIETY OF CHEMISTRY

rsc.li/pccp

View Article Online
DOI: 10.1039/D5CP04347F

ARTICLE

Analysis of Metal-assisted Chemical Etching for Microscale Si Structures Using Arrhenius Method

Received 00th January 20xx,
Accepted 00th January 20xx

DOI: 10.1039/x0xx00000x

Sunhae Choi‡[a], Haekyun Bong‡[a,b], Kyunghwan Kim[c], Sumin Jeon[d], and Jungwoo Oh[a,b,*]

Metal-assisted chemical etching (MACE) has emerged as a promising method for fabricating high-aspect-ratio Si microstructures without the damage or complexity associated with plasma-based etching. However, its thermal activation behavior and the role of catalyst morphology remain poorly understood, especially at the microscale. This study systematically investigated the effects of etchant temperature, metal thickness, and pattern geometry on the etching kinetics of MACE. By constructing Arrhenius plots from etch depth data, activation energies were extracted under various catalyst conditions, revealing that both metal coverage and thickness significantly influence the thermal energy barrier. Notably, an activation energy as low as 20.02 kJ/mol was achieved, which is substantially lower than that of conventional wet etching (>50 kJ/mol), highlighting the efficiency of catalytic charge injection and transport in MACE. This quantitative analysis provides new insights into the fundamental mechanism of MACE and offers practical guidance for optimizing microscale three-dimensional Si fabrication processes.

Introduction

The demand for high-frequency electronic and photonic devices continues to grow, driving the development of advanced three-dimensional (3D) semiconductor architectures such as through-Si vias [1] and trench gate structures [2]. These architectures require the precise etching of Si with high verticality and throughput. Although conventional dry etching methods, such as deep reactive ion etching [3], can produce vertical profiles, they are limited by high processing costs and plasma-induced substrate damage [4]. In contrast, wet etching techniques offer simpler and lower-cost processes with minimal surface damage; however, they lack directionality owing to their inherently isotropic nature. These limitations hinder the efficient fabrication of complex 3D Si microstructures.

To address these challenges, metal-assisted chemical etching (MACE) has been introduced as a promising wet etching technique for fabricating high-aspect-ratio Si structures through solution-based redox reactions [5–7]. In MACE, a patterned noble metal catalyst (typically Au or Ag) deposited on the Si substrate promotes the reduction of an oxidant (e.g., H_2O_2), generating hole carriers (h^+) at the metal surface. These holes are injected into the underlying Si, where they oxidize the Si atoms. The oxidized Si is then selectively dissolved by an acid (e.g., HF), resulting in directional etching beneath the metal layer [8]. This catalytic mechanism produces anisotropic profiles without plasma damage, making MACE attractive for applications in microelectromechanical systems (MEMS) and photonic devices [9,10]. Furthermore, its compatibility with low-cost large-area processing has extended its use beyond Si to compound semiconductors [11] and optoelectronic components [12].

MACE is driven by two coupled electrochemical reactions. At the cathode, the metal surface catalyzes the reduction of H2O2 in the presence of protons, producing h^+, as shown in reaction (1). These holes are injected into the Si underneath the metal, where oxidation occurs. Subsequently, the oxidized Si is dissolved by HF through the anodic reaction in (2), producing soluble byproducts such as hexafluorosilicic acid (H_2SiF_6). As etching occurs only beneath the metal catalyst, this process yields anisotropic profiles. This mechanism minimizes substrate damage and supports the formation of 3D nano/microstructures [8]

(1) Cathode reaction (at metal surface):

$$H_2O_2 + 2H^+ \rightarrow 2H_2O + 2h^+$$
$$2H^+ \rightarrow H_2 + 2h^+$$

(2) Anode reaction (at semiconductor surface):

$$Si + 4h^+ + 4HF \rightarrow SiF_4 + 4H^+$$
$$SiF_4 + 2HF \rightarrow H_2SiF_6$$

The generation and injection of h^+ is referred to as the carrier-generation step, whereas the subsequent transport and removal of the etched byproducts are governed by mass transport. Both steps critically affect the etching rate and profile fidelity. Therefore, understanding and controlling these charge- and mass-transfer mechanisms is essential for optimizing MACE performance [13].

[a] School of Integrated Technology, Yonsei University, Incheon 21983, Republic of Korea.
[b] BK21 Graduate Program in Intelligent Semiconductor Technology, Yonsei University, Incheon 21983, Republic of Korea.
[c] Center for Quantum Technology, Korea Institute of Science and Technology, Seoul 02792, Republic of Korea
[d] Department of Chemistry, Yonsei University, Seoul 03722, Republic of Korea
‡ These authors made equal contributions
* Corresponding Author: jungwoo.oh@yonsei.ac.kr

Numerous studies have sought to optimize MACE by tuning parameters that influence either carrier generation or mass transport processes. For instance, oxidant concentration and metal type have been modified to control hole injection efficiency [14,15], whereas catalyst pattern size and thickness have been varied to regulate the diffusion and removal of byproducts [6,7,16]. Although these approaches have successfully enabled the fabrication of vertically aligned nanostructures, the application of MACE to microscale structures—on the order of several micrometers—remains less effective owing to limited mass transport across larger catalyst areas [15,17,18].

In particular, although it is known that the etching rate depends on temperature, the underlying mechanism by which temperature affects charge and mass transport remains unclear [19]. More importantly, little to no systematic effort has been made to analyze the thermal activation behavior of MACE using Arrhenius analysis. Previous reports did not explicitly address the effects of catalyst thickness or pattern geometry on activation energy [17]. This gap prevents a complete understanding of how physical catalyst parameters influence the thermodynamic behavior of the etching process, which is critical for optimizing microscale process.

This study aims to clarify the thermally activated mechanisms of MACE by systematically analyzing etching kinetics based on Arrhenius behavior. Specifically, it investigated how variations in etchant temperature, catalyst thickness, and pattern geometry influence the activation energy of the etching process. While prior studies have qualitatively reported temperature-dependent changes in etch rate, our approach provides a quantitative framework to extract activation energies and demonstrate their dependence on physical catalyst parameters.

To this end, we performed controlled MACE experiments over a wide range of temperatures by systematically varying metal thicknesses and pattern dimensions. Arrhenius plots constructed from the resulting etch depth data were used to derive the apparent activation energies for each condition. This approach enables the decoupling of charge-transfer and mass-transport contributions to the etching kinetics at the microscale. The insights gained from this analysis offer a deeper understanding of the governing factors in MACE and provide practical guidance for optimizing process parameters for microscale 3D Si fabrication, including applications in Si-based MEMS [20] and micro-total analysis systems [21].

Results and discussion

Before presenting the temperature-dependent morphologies, this study briefly defines the baselines and metrics used. Stripe and dot-mesh patterns with controlled metal coverage (MC) were prepared, the Au thickness was systematically varied, and the etchant composition and etch time were fixed. A mid-thickness Au film was chosen as the baseline to balance etch rate and profile fidelity. The etch rate was obtained from cross-sectional FE-SEM images, while surface quality was determined using atomic force microscopy (AFM). Figure 1 shows the

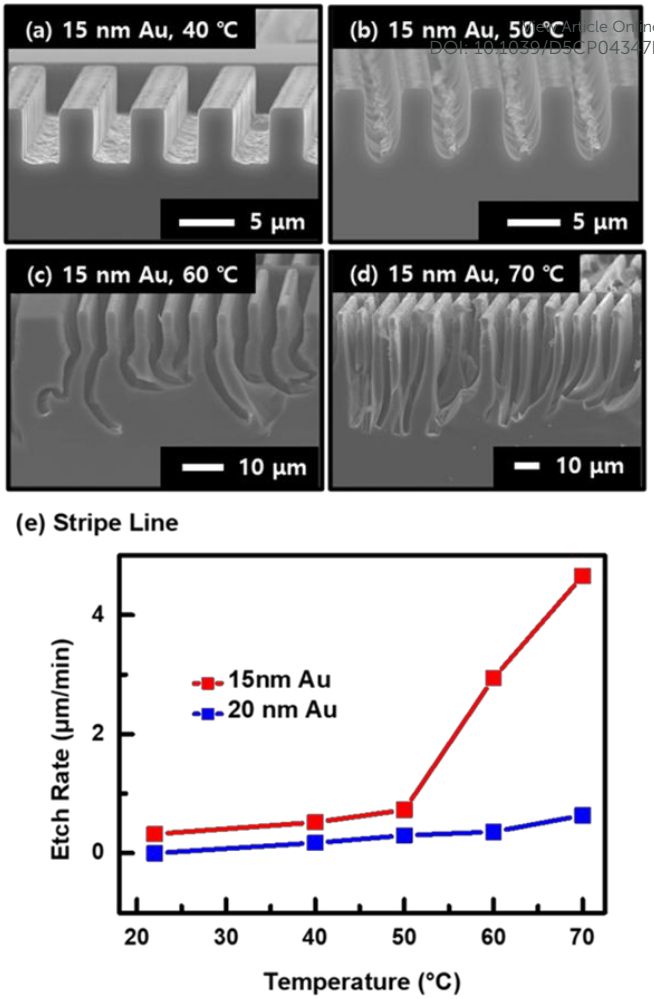

Figure 1 FE-SEM cross-sectional images of line-pattern Si etching at (a) 40 ℃, (b) 50 ℃, (60 ℃, and (d) 70 ℃ with an Au layer thickness of 15 nm. (e) Corresponding etch rate plo for Au layer thicknesses of 15 and 20 nm.

temperature response under this baseline condition, which provides the kinetic input for the subsequent Arrhenius analysis and serves as the basis for analyzing the effects of MC and thickness on activation energy.

To examine the temperature dependence of the MACE mechanism, the etching behavior of Si microstructures was evaluated under varying etchant temperatures using a fixed Au catalyst thickness of 15 nm, previously identified as optimal based on the tradeoff between etch rate and profile fidelity. As shown in Figs. 2(a–d), increasing the etchant temperature from 40 °C to 70 °C significantly enhanced the etch rate, reaching up to 4.66 μm/min at 70 °C. However, at elevated temperatures (≥60 °C), structural deformations and lateral undercutting were observed, indicating catalyst movement caused by non-uniform interface conditions. This transition highlights that etch profile stability in MACE is strongly governed by process parameters, particularly temperature.

These results clearly demonstrate thermal activation of the MACE process in the microscale regime. At the same time, the preservation of pattern-defined vertical profiles below 60 °C indicates that MACE enables controllable and directional

View Article Online
DOI: 10.1039/D5CP04347F

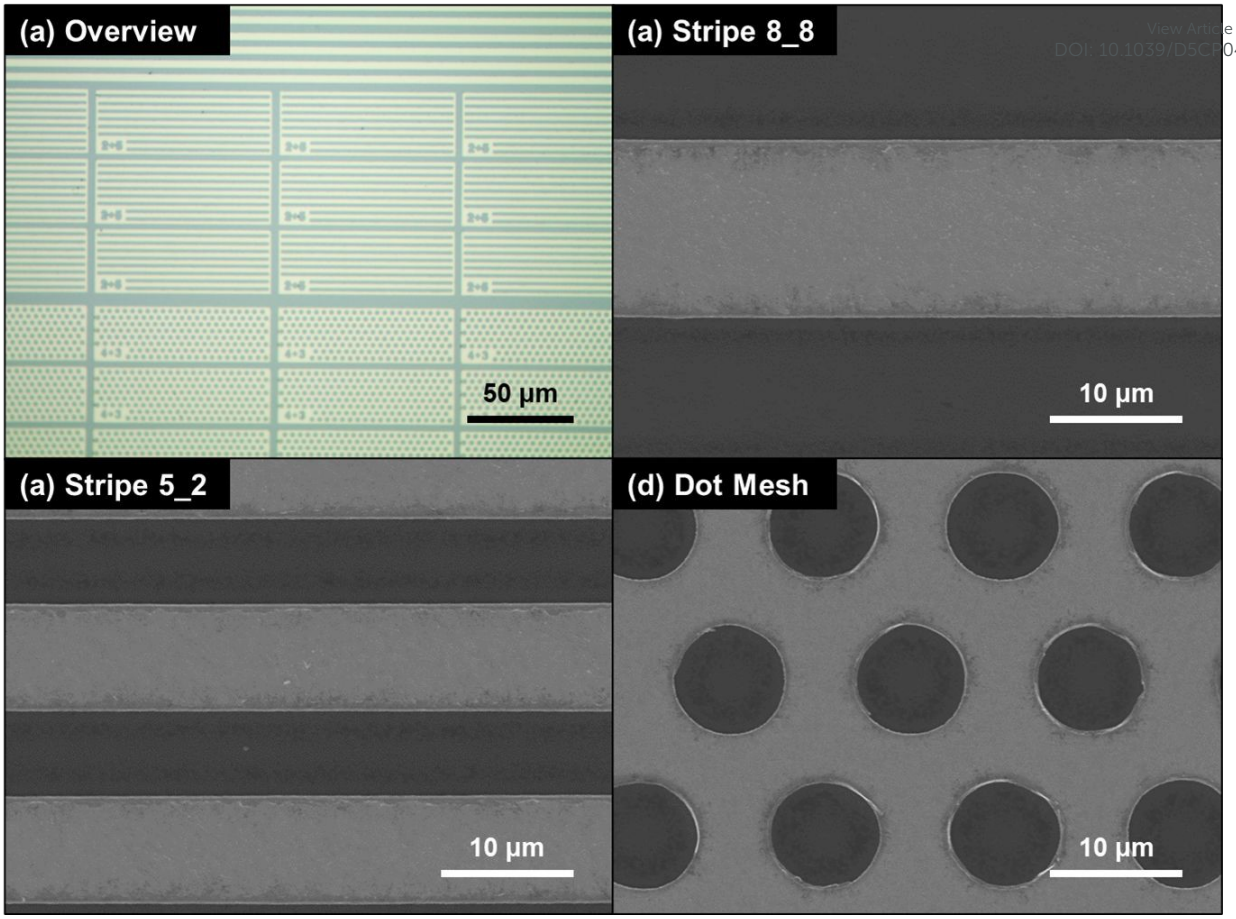

Figure 2 (a) OM overview image showing the full layout of the stripe and dot-mesh Au catalyst patterns. (b) SEM cross-section of the Stripe 8_8 pattern, (c) SEM cross-section of the Stripe 5_2 pattern, and (d) SEM top-view of the dot-mesh pattern. All patterns were etched under identical conditions, and differences in etch depth and verticality are observed depending on the pattern geometry.

etching within a well-defined temperature window. The enhanced redox activity at higher temperatures likely accelerated hole injection and gas evolution at the metal/Si interface, leading to uneven etch progression. Based on this temperature-dependent etching behavior, an Arrhenius analysis approach was adopted to quantitatively extract the activation energies and systematically evaluate how they are affected by metal catalyst parameters such as thickness and pattern geometry. Here, the Arrhenius analysis is used to probe the dominant thermally activated contribution to the etching kinetics within the explored temperature window, rather than to imply a purely kinetic regime. This methodology provides a deeper understanding of the catalytic and transport mechanisms governing microscale MACE.

To evaluate the influence of catalyst pattern geometry and metal coverage (MC), three representative Au configurations were prepared: Stripe 8_8 (MC ≈ 50%), Stripe 5_2 (MC ≈ 71%), and a dot-mesh pattern (MC ≈ 80%). As shown in Fig. 2, all patterns were uniformly transferred onto the Si substrate, confirming consistent catalyst definition across the different geometries. Since each sample was etched under identical conditions, the comparison of pattern design and MC effects on the MACE process can be made on an equal and controlled basis. It should be noted that MC and pattern geometry are partially coupled in this design set, as the highest MC (≈80%) is implemented using a dot-mesh pattern.

This trend can be attributed to enhanced h^+ generation and distribution in patterns with larger catalyst coverage. Since h^+ are generated at the catalyst surface through the reduction of H_2O_2, a higher metal area provides a greater catalytic interface for redox activity, resulting in more efficient carrier injection into the Si substrate. Furthermore, the dot-mesh geometry ensured a high degree of catalyst interconnectivity, which stabilized the reaction front and suppressed catalyst detachment. In the present design, this effect coincides with increased MC, making the two factors difficult to fully decouple. The continuous mesh structure also facilitated uniform lateral current flow and balanced mass transport. In contrast, the solid stripe pattern has a smaller catalyst area and less interconnected geometry, which limited both hole generation rate and the diffusion of etchant species, thereby leading to slower etching and increased non-uniformity. These results highlight the critical role of lateral catalyst design, not only in electrical or mechanical aspects but also in governing redox and transport dynamics at the microscale.

To quantitatively assess the influence of catalyst geometry on etching kinetics, the parameter MC was introduced, defined as the ratio of catalyst-covered area to the total pattern area. Arrhenius plots were constructed for three distinct patterns—

View Article Online
DOI: 10.1039/D5CP04347F

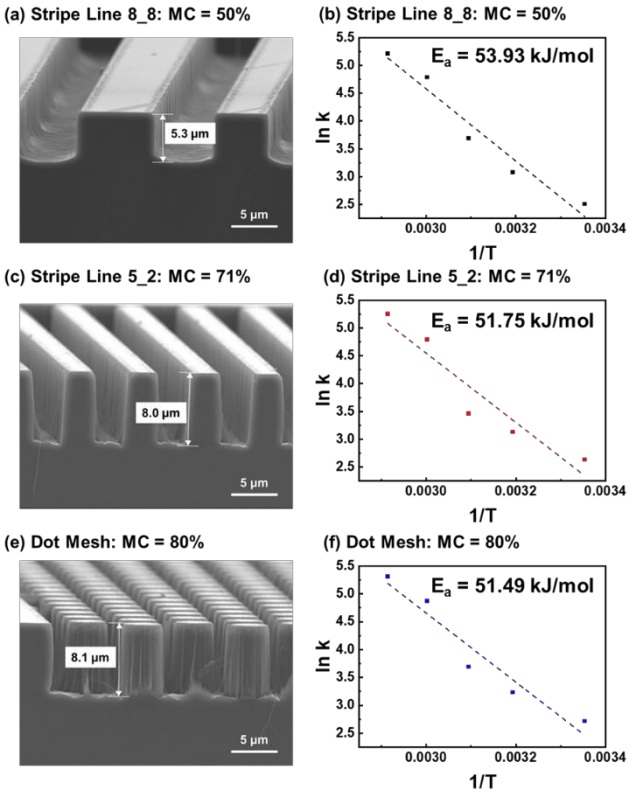

Figure 3 Arrhenius plots of Si etch rate for three catalyst patterns with varying MC: solid stripe (MC ≈ 50%), stripe mesh (MC ≈ 71%), and dot mesh (MC ≈ 80%). The activation energy decreases with increasing MC, indicating more efficient carrier injection and redox reaction at higher MC.

solid stripe (MC ≈ 50%), stripe mesh (MC ≈ 71%), and dot mesh (MC ≈ 80%)—to extract the apparent activation energy (E a) for each case. As shown in Fig. 3, E_a decreased systematically with increasing MC; the solid stripe exhibited the highest E_a, whereas the dotted mesh showed the lowest.

This trend indicates that higher catalyst coverage facilitates more efficient redox reactions by providing a larger interface for hole generation. With increasing MC, h^+ are generated more uniformly and abundantly at the catalyst surface, reducing the thermal barrier required to initiate the etching reaction. Moreover, a higher MC is likely to improve local current distribution and stabilize the reaction front, further lowering the energy required for charge transfer and oxidation. These results suggest that MC is a critical design parameter in MACE that not only influences the etch rate but also acts as a primary descriptor of the effective catalytic area density within the present pattern set. The systematic dependence of E_a on MC further suggests that interfacial catalytic processes make a dominant contribution to the apparent activation barrier, beyond simple mass-transport limitation.

To investigate the effect of catalyst thickness on the thermal activation behavior of MACE, Arrhenius plots were analyzed for samples etched with different Au layer thicknesses (5, 10, 15, and 20 nm). As shown in Fig. 4, the apparent activation energy E_a increases with Au thickness, indicating a less thermally favorable etching process at higher metal thicknesses.

This trend can be explained by changes in both mass transport pathways and the redox reaction environment at the metal/Si

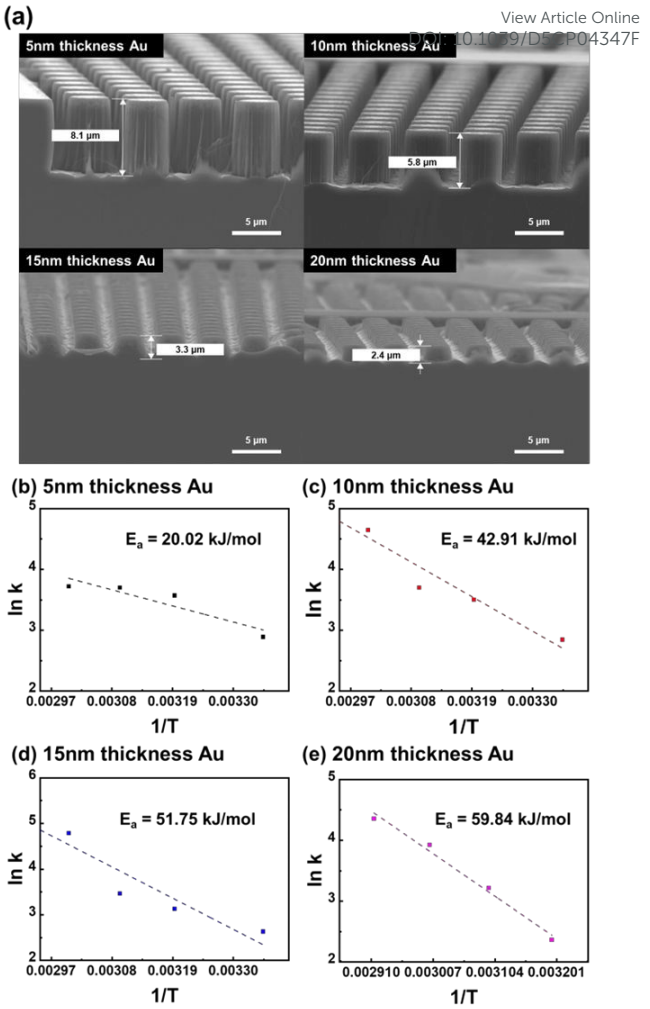

Figure 4 Arrhenius plots of Si etching with different Au catalyst thicknesses (5, 10, 15, and 20 nm). The apparent activation energy E_a increases with catalyst thickness, indicating that thicker Au layers hinder mass transport and raise the energy barrier for the MACE reaction.

interface. Thin Au layers (e.g., 5–10 nm) tend to exhibit a nanoporous morphology, especially after immersion in the etchant, which allows out-of-plane transport of reactants and byproducts through pinholes. This promotes efficient delivery of h^+ and facilitates the removal of etch byproducts, thereby reducing the energy barrier for the overall etching reaction. In contrast, thicker Au layers (≥20 nm) form more continuous and denser films that suppress these vertical diffusion paths. Consequently, etching becomes increasingly reliant on lateral mass transport along the metal/Si interface, which is inherently less efficient. This shift from a mixed-transport regime to one dominated by lateral diffusion leads to a higher energy barrier, reflected in the increased activation energy observed for thicker catalysts. This behavior indicates a reduced contribution from interfacial kinetic enhancement as transport limitations become more pronounced.

Furthermore, the extracted activation energies provide clear evidence of the superiority of MACE over conventional wet etching. In typical wet etching of Si, the activation energies often exceed 50 kJ/mol because of the isotropic nature of the process and the inefficient mechanisms of hole generation [22]. In contrast, optimized MACE conditions achieved activation

View Article Online
DOI: 10.1039/D5CP04347F

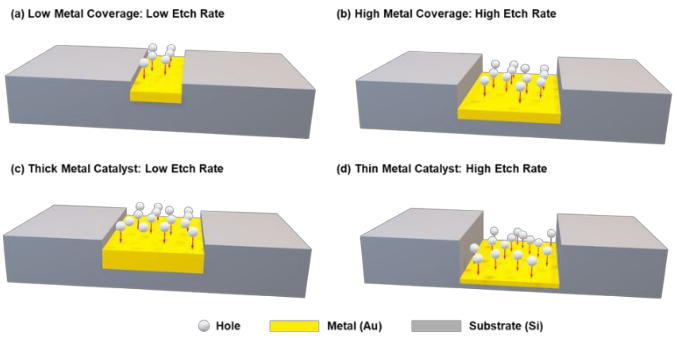

Figure 5 Schematic of MACE mechanisms. (a, b) Higher MC enhances hole generation, thereby increasing the etch rate. (c, d) Thin catalysts allow vertical hole diffusion, while thick films block it, reducing etch efficiency.

energies as low as 20.02 kJ/mol. This significant reduction in the energy barrier results from the catalytic role of the metal, which locally enhances carrier generation via surface redox reactions and facilitates vertical charge injection into the Si substrate. These activation energies therefore represent effective barriers under the present MACE conditions, reflecting the combined influence of interfacial kinetics and transport processes. Additionally, the engineered thin and porous catalyst morphology promotes efficient mass transport of etching byproducts and reactants, further lowering the energy requirement for etching. These results demonstrate that MACE is a more energetically favorable and directional etching process for microscale Si structures.

To further clarify how catalyst design influences etching behavior in MACE, a schematic model was developed to illustrate two key design parameters: (1) MC area and (2) metal thickness (Fig. 5). In the first case (a,b), an increase in MC enhances the density of available catalytic sites for H_2O_2 reduction, thereby increasing h^+ generation. This facilitates a more uniform and rapid injection of holes into the Si substrate, leading to a higher etching rate. Conversely, low MC yields limited hole generation and uneven charge distribution, which slows the reaction and introduces etch non-uniformity.

In the second case (c, d), the thickness of the metal catalyst determines the mass transport efficiency. Thin Au films (~5–10 nm) tend to become semi-porous under etching conditions, enabling the vertical transport of reactants and byproducts through pinholes. This promotes efficient out-of-plane diffusion and reduces the activation barrier for etching. In contrast, thick and dense metal layers (e.g., ≥ 20 nm) block vertical transport and force byproducts to diffuse laterally along the metal/Si interface. This shift to a lateral diffusion-dominated regime reduces etching efficiency and increases the apparent activation energy. These schematic models support the experimental findings and provide a conceptual framework for rational catalyst design in MACE.

To evaluate the surface quality of the etched structures, AFM measurements were performed after MACE under varying temperatures. As shown in Fig. 6, the RMS roughness remained relatively low from room temperature to 50 °C, with the initial value at room temperature measured at 1.610 nm. However, a sharp increase in surface roughness was observed at 60 °C,

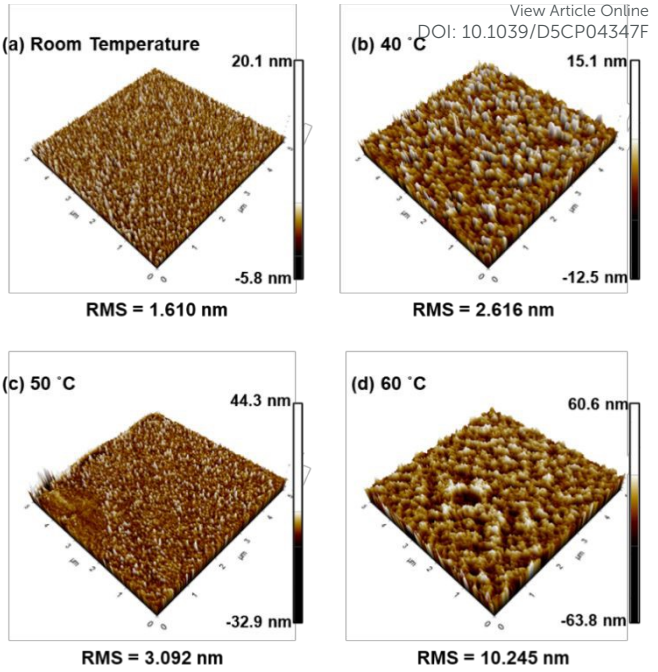

Figure 6 AFM topography images of Si surfaces etched via MACE at (a) Room temperature, (b) 40 °C, (c) 50 °C, and (d) 60 °C. Root mean square (RMS) roughness remained low up to 50 °C (1.610 nm at room temperature) but increased sharply at 60 °C and above, indicating thermally induced surface degradation.

indicating the onset of etch instability. This transition corresponded to the etch profile collapse and catalyst detachment phenomena previously observed in the FE-SEM analysis. These results suggest that although elevated temperatures accelerate the etching rate, they can also induce undesirable surface degradation. Therefore, maintaining the etchant temperature below 60 °C enables MACE to achieve both high etch rates and excellent surface smoothness—an advantage over traditional wet etching techniques, which typically struggle to balance speed and surface quality. Therefore, maintaining the etchant temperature below 60 °C enables MACE to achieve both high etch rates and excellent surface smoothness- while preserving pattern-defined etch profiles, an advantage over traditional wet etching techniques, which typically struggle to balance speed, surface quality, and profile fidelity.

Experimental

B-doped p-type Si(100) substrates with resistivities of 5–10 Ω·cm were used. The Si substrates were precleaned by immersion in $(CH_3)_2CO$, C_3H_8O, and deionized (DI) water for 2 min each. Stripe-line patterns (2 µm-wide Si stripes with a metal spacing of 5 µm) and dot-mesh patterns (Si dots with 4-µm diameter and 3-µm metal spacing) were photoresist-patterned using image-reversal optical lithography. The substrates were immersed in a buffered oxide etchant to remove the native oxide and rinsed in DI water before metal deposition. An Au layer was deposited onto each substrate via thermal evaporation at a rate of 2 Å/s under a pressure of 10–6 Torr. Au layers of 5–30 nm thickness were deposited, followed by a lift-off

process. The etching solution, consisting of 4 mL H2O2 as the oxidant, 20 mL HF, and 90 mL DI water, was stirred for 30 min. The etchant temperature was varied from room temperature to 70 °C, and all samples were etched for a fixed time of 10 min. After etching, the samples were thoroughly rinsed with DI water and dried under an N2 stream. The etch depths were measured using field-emission scanning electron microscopy (FE-SEM), and the etch rate was calculated based on the height of the etched structure and etching time.

Conclusions

This study systematically investigated the thermal activation behavior of the MACE process for microscale Si structures by controlling catalyst thickness, pattern geometry, and etching temperature. Through Arrhenius analysis of experimental etch rates, activation energies were quantitively extracted, revealing the critical influence of catalyst morphology on etching kinetics and verticality. A key finding was the significant reduction of activation energy to 20.02 kJ/mol—substantially lower than that of conventional wet etching (~50 kJ/mol). This reduction is attributed to the catalytic role of the metal, which enhances localized charge injection and facilitates mass transport, especially in thin and porous metal layers. Greater MC and reduced thickness further lowered the energy barriers by promoting efficient hole injection and byproduct removal. While previous studies have focused mainly on qualitative trends, the present results provide a quantitative framework linking catalyst design to thermodynamic behavior. These findings offer practical guidance for optimizing MACE processes to achieve high etch rates with excellent surface quality, particularly in microscale applications where transport effects are critical.

Author contributions

S. Choi and H. Bong contributed equally to this work. S. Choi, H. Bong and J. Oh developed the original ideas. S. Choi and S. Bong carried out the experimental work. S. Choi, H. Bong and J. Oh contributed to the paper writing. K. Kim and S. Jeon assisted with some data analysis. All authors have given approval to the final version of the manuscript.

Conflicts of interest

There are no conflicts to declare.

Acknowledgements

This research work was supported by the BK21 FOUR (Fostering Outstanding Universities for Research) funded by the Ministry of Education (MOE) of Korea and National Research Foundation (NRF) of Korea. This research work was also supported by the National Research Foundation of Korea (NRF) grant funded by the Ministry of Science and ICT of Korea (RS-2024 00344625). This research was supported by Korea Institute for Advancement of Technology (KIAT) grant funded by the Korea Government (Ministry of Education) (P0028089, "Semiconductor" -Specialized University).

View Article Online DOI: 10.1039/D5CP04347F

Notes and references

1 Guo, Haoming, et al., Materials Science in Semiconductor Processing, 2022, **137**, 106182
2 Williams, Richard K., et al., *IEEE Transactions on Electron Devices*, 2017, **64.3**, 674-691.
3 Waits, C. M., et al., *Sensors and Actuators A: Physical*, 2005, **119.1**, 245-253.
4 Fonash, Stephen J., *Journal of The Electrochemical Society*, 1990, **137.12**, 3885.
5 Kim, Kyunghwan, et al., *Advanced Optical Materials*, 2020, **8.15**, 2000143.
6 Choi, Keorock, et al., *RSC advances*, 2015, **5.93**, 76128-76132.
7 Choi, Keorock, et al., *ACS omega*, 2017, **2.5**, 2100-2105.
8 Huang, Zhipeng, et al., *Advanced materials*, 2011, **23.2**, 285-308.
9 Ki, Bugeun, et al., *Scientific reports*, 2020, **10.1**, 1-9.
10 Ki, Bugeun, et al., *Nanoscale*, 2020, **12.11**, 6411-6419.
11 Kim, Kyunghwan, et al., *ACS nano*, 2019, **13.11**, 13465-13473.
12 Choi, Keorock, et al., *Nanoscale*, 2019, **1.32**, 15367-15373.
13 Kim, Jeong Dong, et al., *Advanced Functional Materials*, 2017, **27.12**, 1605614.
14 Hildreth, et al., *ACS nano*, 2009, **3.12**, 4033-4042.
15 Kim, Sang-Mi, and Dahl-Young Khang., *Small*, 2014, **10.18**, 3761-3766.
16 Nur'aini, Anafi, and Ilwhan Oh., *ACS omega*, 2022, **7.19**, 16665-16669.
17 Um, Han-Don, et al., *Scientific reports*, 2015, **5.1**, 1-11.
18 Romano, Lucia, et al., *Rsc Advances*, 2016, **6.19**, 16025-16029.
19 Backes, Andreas, et al., *ECS Journal of Solid State Science and Technology*, 2016, **5.12**, P653.
20 Khatokar, J. Aditya, et al., *Materials Today: Proceedings*, 2021, **43**, 784-3790.
21 Patabadige, Damith EW, et al., *Analytical chemistry*, 2016, **88.1**, 320-338.
22 Gondek, Christoph, et al., *The Journal of Physical Chemistry C*, 2014, **118.4**, 2044-2051.

View Article Online
DOI: 10.1039/D5CP04347F

Data Availability

All data generated or analyzed during this study are included in this published article and its Supplementary Information.